

## Continuous-time random-walk model of transport in variably saturated heterogeneous porous media

Andrea Zoia,<sup>1,\*</sup> Marie-Christine Néel,<sup>2</sup> and Andrea Cortis<sup>3</sup>

<sup>1</sup>*DEN/DM2S/SFME/LSET, CEA Saclay, Bât. 454, 91191 Gif-sur-Yvette Cedex, France*

<sup>2</sup>*Université d'Avignon et des Pays de Vaucluse, UMR 1114 EMMAH, 84018 Avignon Cedex, France*

<sup>3</sup>*Earth Sciences Division, Lawrence Berkeley National Laboratory, Berkeley, California 94720, USA*

(Received 16 October 2009; published 4 March 2010)

We propose a unified physical framework for transport in variably saturated porous media. This approach allows fluid flow and solute migration to be treated as ensemble averages of fluid and solute particles, respectively. We consider the cases of homogeneous and heterogeneous porous materials. Within a fractal mobile-immobile continuous time random-walk framework, the heterogeneity will be characterized by algebraically decaying particle retention times. We derive the corresponding (nonlinear) continuum-limit partial differential equations and we compare their solutions to Monte Carlo simulation results. The proposed methodology is fairly general and can be used to track fluid and solutes particles trajectories for a variety of initial and boundary conditions.

DOI: [10.1103/PhysRevE.81.031104](https://doi.org/10.1103/PhysRevE.81.031104)

PACS number(s): 05.40.Fb, 66.10.cg, 05.60.Cd

### I. INTRODUCTION

Accurately predicting the spreading of a chemical species through unsaturated porous materials (i.e., materials with locally varying fluid content) is key to mastering such technological challenges as polluted sites remediation, environmental protection, and waste management [1–6]. The evolution of the solute concentration profile in the traversed medium cannot be *a priori* decoupled from that of the fluid flow, which is ultimately responsible for the advection and dispersion mechanisms of the solutes. Moreover, the effects of the fluid distribution are often combined with those of spatial heterogeneities. Such heterogeneities can be present both at the pore scale (microscopic) and at the Darcy scale (macroscopic). As a consequence, experimental results reported in literature often show that solutes concentration displays non-Fickian features, such as breakthrough curves with long tails and non-Gaussian spatial profiles [6–8].

In this respect, there exists an increasing need for reliable numerical techniques to tackle flow and transport problems. In this work, we address the issue of determining the fluid content and the solute concentration profiles within unsaturated homogeneous as well as heterogeneous media by resorting to a random-walk approach. Random walks are extensively used to describe solutes transport in saturated media [9], although their application to unsaturated flows appears to be somehow neglected [10]. While complementing each other, the random walk and the continuum-limit approaches display specific advantages and disadvantages. Random walks, for instance, do not introduce the spurious numerical dispersion typical of Eulerian (continuum) numerical schemes [9–11]. As such, random walks are particularly well suited to deal with unsaturated materials, where sharp contrasts between stagnant and fluid-saturated regions, or at macroscopic heterogeneity interfaces, may give rise to steep propagating fronts. Eulerian (continuum) numerical schemes,

on the other hand, are generally faster than the corresponding Monte Carlo simulations.

We begin our analysis by illustrating flow and transport in homogeneous media and detail how the Richards equation for the fluid flow and the advection-dispersion equation (ADE) for the solutes can be recast in a Fokker-Planck equation (FPE) form. The FPE governs the probability density (pdf) of finding a walker (a fluid or solute parcel, respectively) at a given position at a given time. The central idea is that these walkers perform stochastic trajectories in the traversed medium. Taking the ensemble average of the fluid and solute parcel trajectories yields the desired macroscopic quantities, i.e., the fluid content and solutes concentration profiles. As the fluid movement and the solute transport are (nonlinearly) coupled via the macroscopic governing equations, the underlying stochastic trajectories also display a nonlinear coupling. On the other hand, the homogeneity hypothesis ensures that the trajectories carry no memory of the past, so that the particles dynamics is Markovian [12].

Then, we focus our attention on unsaturated heterogeneous materials, where non-Fickian behaviors are enhanced by the interplay between nonlinearities in the flow patterns and complex spatial structures: the relative strength of these processes determines the precise details of the solutes distribution. We model the effects of complex nonhomogeneous spatial structures by introducing the possibility of trapping events between successive particles displacements, as customary within a continuous time random-walk (CTRW) approach [13–15]. The resulting broad distribution of waiting times at each visited site characterizes the broad velocity spectrum that is often observed in heterogeneous media.

This paper is organized as follows. In Sec. II, we review the equations that govern the coupled flow-transport problem for nonstationary variable-saturation conditions. Then, in Sec. III, we present a general nonlinear random-walk approach to the simulation of fluid and contaminant particles in locally homogeneous media. These simulation schemes are compared to numerical solutions of the governing equations in Sec. IV for a variety of initial and boundary conditions.

\*andrea.zoia@cea.fr

The case of discontinuous physical properties of the traversed media is addressed as well. In Sec. V, we extend our results to heterogeneous porous media and derive the corresponding macroscopic governing equations. Finally, conclusions are drawn in Sec. VI.

## II. GOVERNING EQUATIONS IN UNSATURATED HOMOGENEOUS MEDIA

In the following, we shall briefly review the equations that govern nonstationary flow-transport processes in unsaturated homogeneous porous media. Consider a vertical column of length  $\ell$  and radius  $r \ll \ell$  so that the flow-transport process can be considered one dimensional along the longitudinal direction. Let the column be filled with a homogeneous porous material and suppose that the medium has an initial variable saturation. The fluid flow dynamics within such region can be described in terms of the (dimensionless) volumetric fluid content  $0 < s(x, t) < 1$ , which is defined as the ratio between the volume occupied by the fluid and the total volume (water, soil and voids) [3,12]. The medium saturation is then given by the ratio of the volumetric water content and porosity. When  $s(x, t) = 1$  everywhere, the medium is fully saturated in fluid (to the extent granted by porosity). The upper limit to saturation is naturally set by the medium porosity, i.e., by the volume fraction that is actually viable to the fluid.

The evolution of the volumetric fluid content is ruled by the continuity equation

$$\partial_t s(x, t) = -\partial_x j_s(x, t), \quad (1)$$

provided that the porosity is constant, i.e., the soil skeleton is rigid [16]. The so-called Buckingham-Darcy flux (or generalized Darcy's law)  $j_s(x, t)$  [ $L/T$ ] is provided by the constitutive equation

$$j_s(x, t) = K(s)[1 - \partial_x h(s)], \quad (2)$$

where the quantity  $K(s)$  [ $L/T$ ] is the saturation-dependent hydraulic conductivity and  $h(s)$  [ $L$ ] is the saturation-dependent capillary pressure [3,12]. The capillary head depends on soil pore size. In sandy soils with larger pores, the head will be less than in clay soils with very small pores. Then, by introducing the capillary diffusivity  $\kappa(s) = K(s) \partial h / \partial s$  [ $L^2/T$ ], we can combine Eqs. (1) and (2) so to obtain

$$\partial_t s(x, t) = \partial_x \kappa(s) \partial_x s(x, t) - \partial_x K(s). \quad (3)$$

In this form, Eq. (3) has been first derived by Richards [17]. Observe that within this framework, one single phase is considered, i.e., that of the fluid which evolves through the pore structure of the medium. Other models involve the coexistence of several fluid phases (with exchanges between phases), but we do not address this issue here. The Richards equation has been extensively adopted in describing the dynamics of fluid flows during wetting processes in soils (see the discussion in [16] and references therein).

Without loss of generality, we can finally put Eq. (3) in conservative form by conveniently defining a "velocity"  $v(s) = K(s)/s$  [ $L/T$ ],

$$\partial_t s(x, t) = -\partial_x [v(s) - \kappa(s) \partial_x] s(x, t). \quad (4)$$

The term  $v(s)$  plays the role of an effective velocity for the fluid particles and represents the gravitational contribution to the flow dynamics. Remark that Eq. (4) is nonlinear, in that the diffusion  $\kappa(s)$  and advection  $v(s)$  coefficients depend in general on  $s$ . In some special cases, it is nonetheless possible to obtain analytical solutions by resorting to the scaled (Boltzmann) variable  $\epsilon = xt^{-1/2}$  [16,18].

Flow dynamics must be supplemented by the initial and boundary conditions. To set the ideas, as a representative example, we may impose  $s(0, t) = 1$ , i.e., we keep the inlet on the column at a constant full saturation. This condition may be physically achieved by putting the porous column in contact with a fluid reservoir (infiltration process). Along the column, we initially assign a given saturation distribution, for instance, a constant profile  $s(x, 0) = s_0$ , for  $x > 0$ . Finally, at the outlet of the column, we prescribe a vanishing diffusive flux,  $\partial_x s(x, t)|_{x=\ell} = 0$  (Neumann boundary condition), i.e., a flat concentration profile.

We assume now that a (nonreactive) tracer, e.g., some chemical species, flows diluted in the fluid which is injected into the porous column. Provided that the medium is sufficiently homogeneous and that physical-chemical interactions of the transported species with the porous matrix and preferential flows can be excluded [19,20], the solutes dynamics obeys an ADE with saturation-dependent coefficients

$$\partial_t s c(x, t) = -\partial_x [u(s) - sD(s) \partial_x] c(x, t), \quad (5)$$

where  $c(x, t)$  is the solutes concentration and  $s = s(x, t)$ .

The advection term  $u(s)$  is determined by the fluid flow, namely,  $u(s) = j_s(x, t)$ , whereas the effective dispersion coefficient  $D(s)$  accounts for the effects of mechanical dispersion and molecular diffusion mechanisms [3]. Note that Eq. (5) is linear, although knowledge of the saturation  $s(x, t)$  is required in order to determine  $c(x, t)$ , i.e., problems (5) and (4) are inherently coupled. Owing to this coupling and to the nonlinearities, the flow patterns are not homogeneous, so that the evolution of the solutes dynamics usually displays non-Fickian features, such as long tails and non-Gaussian shapes. We will discuss this point in details in the next section. When the saturation level is uniform within the column, i.e.,  $s(x, t) = s_0$ , Eq. (5) reduces to a standard ADE with constant coefficients and contaminant transport becomes Fickian.

Concerning initial and boundary conditions for the solute species, in the following, we will assume that contaminant release occurs within a given time interval  $t_0 \leq t \leq t_c$  and that during this time span, the pollutants concentration at the column inlet has a constant value  $c_0$ , i.e.,  $c(0, t_0 \leq t \leq t_c) = c_0$ . Such finite-extension contaminant spills are commonly encountered in environmental remediation problems [3]. Before injection, there is no contaminant within the column, i.e.,  $c(x, t \leq t_0) = 0$ . The boundary condition for the concentration at the outlet is dictated by the outlet boundary for the flow, i.e., it must be a Neumann boundary condition,  $\partial_x c(x, t)|_{x=\ell} = 0$ .

### III. RANDOM-WALK APPROACH

Flow-transport equations (4) and (5) share a similar structure and can be both written in conservative form as

$$\partial_t \theta p(x,t) = -\partial_x [\theta q - \theta d \partial_x] p(x,t) \quad (6)$$

for the evolution of the field  $p(x,t)$ . The coefficients  $\theta = \theta(x,t)$ ,  $q = q(x,t)$ , and  $d = d(x,t)$  are generally space and time dependent. This conceptual picture allows Eqs. (4) and (5) to be expediently solved by resorting to a random-walk formulation. The key idea is to think of the evolving (fluid or contaminant) plume, whose dynamics is described by Eq. (6), as being composed of a large number of particles performing stochastic trajectories in the traversed porous medium. Then, the quantity  $p(x,t) \geq 0$  can be given a probabilistic interpretation (up to a normalization factor), i.e.,  $p(x,t)$  represents the probability density of finding a walker at a given position  $x$  at time  $t$ .

Consider an ensemble of  $N$  particles at positions  $x_j(t)$ ,  $j = 1, \dots, N$ . Assume that the stochastic dynamics of each walker is governed by a Langevin-type equation

$$x_j(t + \tau) = x_j(t) + A(x,t)\tau + \sqrt{2B(x,t)}\tau\xi_j, \quad (7)$$

where  $A(x,t)$  is the drift coefficient, representing the average velocity,  $B(x,t)$  is the diffusion coefficient, and  $\tau$  a (small) time step. The quantity  $\xi_j$  is a white noise with zero mean and unit variance. The coefficients  $A(x,t)$  and  $B(x,t)$  completely define the properties of the microscopic particles dynamics. Remark that Eq. (7) describes a Markovian (memoryless) process: although the evolution of a single trajectory may depend on the others (i.e., the process can in general be nonlinear), knowledge of particles positions at time  $t$  is sufficient to determine the displacements at the following step  $t + \tau$ . It can be shown that the ensemble-averaged density  $P(x,t)$  of a particle plume obeying Eq. (7), i.e.,

$$P(x,t) = \left\langle \sum_j \delta[x - x_j(t)] \right\rangle, \quad (8)$$

satisfies the (in general nonlinear) Fokker-Planck equation [21]

$$\partial_t P(x,t) = -\partial_x [A(x,t) - \partial_x B(x,t)]P(x,t). \quad (9)$$

Nonlinearities arise when  $A = A(P)$  and/or  $B = B(P)$ , i.e., when the coefficients depend on particles concentration.

Then, if we want to identify the walkers in Eq. (7) with the microscopic dynamics underlying Eq. (6), we must properly assign the drift  $A(x,t)$  and diffusion  $B(x,t)$  of the stochastic process. In other words, we must impose  $A(x,t)$  and  $B(x,t)$  so that knowledge of  $P(x,t)$  provides information on the quantity  $p(x,t)$ : this in turn establishes a link between the physical variables  $\theta(x,t)$ ,  $q(x,t)$ ,  $d(x,t)$  and the parameters  $A(x,t)$  and  $B(x,t)$ .

Letting [21]

$$A(x,t) = q(x,t) + \frac{1}{\theta(x,t)} \partial_x \theta(x,t) d(x,t) \quad (10)$$

and

$$B(x,t) = d(x,t), \quad (11)$$

it is easy to prove that

$$p(x,t) = P(x,t)/\theta(x,t) \quad (12)$$

up to a normalization factor, which provides the desired link.

Let us address Eq. (4) first. In this case, the particles that stochastically travel in the porous medium represent fluid parcels that progressively change the saturation distribution in the traversed region [12]. The nonlinearity of the governing equation arises from the fact that the advection and diffusion coefficients depend both on  $s(x,t)$ . Then, determining the evolution of the saturation profile at time  $t + \tau$  requires preliminarily knowing the saturation profile itself at time  $t$ . In terms of random walks, this implies that particle positions at the following time step can be updated once the positions of all the particles at the current time have been determined. In other words, particle trajectories are correlated via the saturation, as the advection and diffusion coefficients depend on the fluid saturation,  $s$ . At each time step  $\tau$ ,  $s(x,t)$  is first computed on the basis of particles positions at time  $t$ , then time is updated  $t = t + \tau$  and particles are displaced. From the previous considerations (the parameter  $\theta$  is assumed to be constant and can be simplified), it follows that

$$x_j^s(t + \tau) = x_j^s(t) + \mu^s + \sigma^s \xi_j, \quad (13)$$

where

$$\mu^s = [v(s) + \partial_x \kappa(s)]\tau \quad (14)$$

and

$$\sigma^s = \sqrt{2\kappa(s)}\tau. \quad (15)$$

In the hydrodynamic limit  $\tau \rightarrow 0$ , the ensemble-averaged fluid parcel profiles  $P_s(x,t)$  converge to the solution  $s(x,t)$  of Eq. (4).

Once  $s(x,t)$  has been obtained at each time step, the evolution of the concentration profile in Eq. (5) can be determined from a second ensemble of particles representing the pollutant parcels. This (linear) random walk must obey

$$x_j^c(t + \tau) = x_j^c(t) + \mu^c + \sigma^c \xi_j, \quad (16)$$

where

$$\mu^c = \left[ \frac{u(s)}{s} + \frac{1}{s} \partial_x s D(s) \right] \tau \quad (17)$$

and

$$\sigma^c = \sqrt{2D(s)}\tau. \quad (18)$$

Finally, we can identify  $c(x,t) = P_c(x,t)/s(x,t)$ , where  $P_c(x,t)$  is the ensemble-averaged concentration of the contaminant walkers.

In principle, the random-walk schemes defined above can be used to determine fluid saturation and contaminant concentration profiles for an arbitrary choice of the time- and space-dependent coefficients. In practice, however, because of the sharp gradients and steep profiles resulting from the nonlinearities in Eq. (4), special care is needed in the choice of the numerical values for the time step,  $\tau$ . Also, the evalu-

ation of the space derivatives in the drift terms of the random walk is ill-defined for abrupt jumps (discontinuities) in the equations parameters [22–24]. In all such cases, it is convenient to resort to the *ad hoc* scheme originally proposed in [22] for particle transport in composite porous media. For instance, the random walk for the case of fluid parcels would read

$$x_j^s(t + \tau) = x_j^s(t) + v(s)\tau + \sigma^s[x_j^s(t) + \Delta x^s]\xi_j, \quad (19)$$

where

$$\Delta x^s = \sigma^s[x_j^s(t)]\xi_j. \quad (20)$$

The expression for the case of contaminant particles (with nonconstant  $\theta$ ) is more involved and reads as

$$x_j^c(t + \tau) = x_j^c(t) + \frac{u(s)}{s}\tau + \frac{1}{\sqrt{s}}\hat{\sigma}^c[x_j^c(t) + \Delta x^c]\xi_j, \quad (21)$$

where

$$\hat{\sigma}^c = \sqrt{2D(s)s\tau} \quad (22)$$

and

$$\Delta x^c = \frac{1}{\sqrt{s}}\hat{\sigma}^c[x_j^c(t)]\xi_j. \quad (23)$$

In [22], it has been shown that schemes (19) and (21) are equivalent to Eqs. (13) and (16), respectively, when coefficients are sufficiently smooth.

Finally, just as for the governing equations above, the random-walk schemes must be supplemented by the appropriate boundary and initial conditions. For each scheme separately, at time  $t=0$ , a given (large) number of particles is attributed to each  $dx$  along the discretized domain representing the column, so to reproduce the initial saturation distribution and the contaminant concentration profile. A constant saturation level (or concentration) at the inlet is imposed at each time step by keeping the number of particles located at  $x=0$  equal to some reference value, i.e., by replacing the walkers that have either come back to the reservoir ( $x < 0$ ) or moved toward the interior of the column ( $x > 0$ ). The Neumann boundary condition at the outlet is imposed by applying a reflection rule to the diffusive component of the displacement, while particles advected past the outlet during the same time step are removed from simulation. Note that a Dirichlet (absorbing) boundary condition at the outlet would correspond to removing each particle from the ensemble upon touching the column end.

Given an initial particles configuration, these are displaced at each time step according to the rules prescribed above. First, the necessary coefficients are computed at assigned  $s(x, t)$  profile (which is known on the basis of flow parcels positions). This allows displacing the walkers at position  $x_j^s$  during the time step  $\tau$ . Then, the  $s(x, t)$  profile is updated. Finally, the walkers at position  $x_j^c$  are displaced and their profile updated. Up to a normalization factor, the spatial profiles are determined by ensemble averaging the walker locations at a fixed time; the breakthrough curves at a given position are determined by counting the net number of walkers crossing that location at each time step. Given the non-

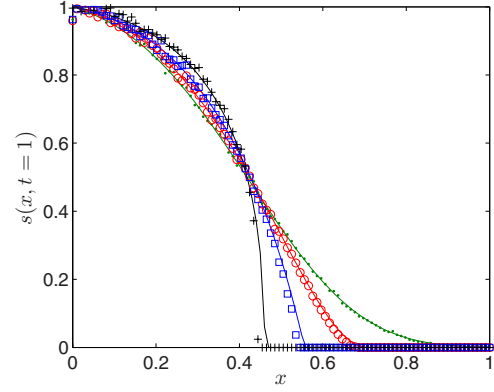


FIG. 1. (Color online) Saturation level spatial profiles  $s(x, t)$  at fixed time  $t=1$  for varying  $\chi$ . Numerical integration of Eq. (4) is displayed as solid lines, Monte Carlo simulation as symbols:  $\chi=0.1$  (green dots),  $\chi=0.5$  (red circles),  $\chi=1$  (blue squares), and  $\chi=2$  (black crosses). The other coefficients are  $\kappa_0=0.05$ ,  $v_0=0.3$ , and  $\nu=0.4$ .

linearities and the coupling between the two schemes, the time step  $\tau$  must be chosen sufficiently small to achieve convergence. Moreover, the number of simulated particles must be sufficiently large to attain a good accuracy in the estimated profiles.

#### IV. NUMERICAL SIMULATIONS AND COMPARISONS

We compare now the Monte Carlo simulations of the random-walk schemes proposed in Sec. III to the numerical solution of the governing equations for  $s(x, t)$  and  $c(x, t)$ . In principle, the random-walk schemes are very general and can account for arbitrary functional forms (even discontinuous) of the various coefficients. In the following examples, we will focus on a power-law scaling, which is commonly encountered in the empirical constitutive laws, such as the Van Genuchten or Brooks and Corey laws, and can usually fit experimental data [3, 12, 18, 25, 26]. In particular, for the volumetric fluid content, we will assume  $\kappa(s) = \kappa_0 s^\chi$  and  $v(s) = v_0 s^\nu$ ,  $\kappa_0$  and  $v_0$  being some constant reference values. The exponents  $\chi$  and  $\nu$  are material parameters and depend on the details of the microgeometry. Moreover, for the solutes concentration evolution, we also assume power-law scaling,  $D(s) = D_0 s^\phi$ , where  $D_0$  is a constant diffusion coefficient and  $\phi$  is the scaling exponent.

The physical quantities that we examine in the following are the spatial profiles at a fixed time, which are helpful in estimating the average displacement and spread of the fluid flow and of the contaminant species and the breakthrough curves at the outlet of the column, which allow assessing the distribution of the times needed to travel from the source to the measure point. In the following, we assume that the column has unit length,  $\ell=1$ . Furthermore, we assume a constant saturation level  $s(0, t)=1$  at the inlet and let the fluid flow infiltrate the column under the combined action of capillarity and gravity.

Figure 1 shows the influence of the power-law scaling exponent for the capillary diffusivity,  $\chi$ , on the spatial profiles of the fluid saturation,  $s(x, t)$ , at a fixed time  $t=1$

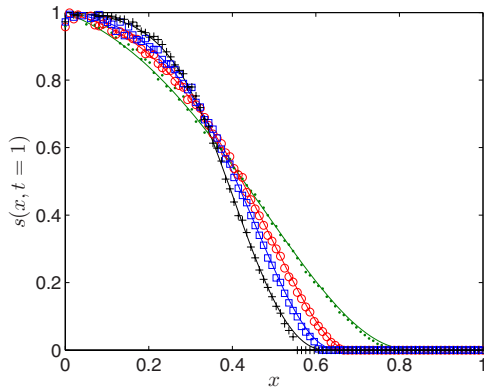


FIG. 2. (Color online) Saturation level spatial profiles  $s(x, t)$  at fixed time  $t=1$  for varying  $\nu$ . Numerical integration of Eq. (4) is displayed as solid lines, Monte Carlo simulation as symbols:  $\nu=0$  (green dots),  $\nu=0.5$  (red circles),  $\nu=1$  (blue squares), and  $\nu=2$  (black crosses). The other coefficients are  $\kappa_0=0.05$ ,  $v_0=0.3$ , and  $\chi=0.5$ .

( $\chi=0.1, 0.5, 1$ , and  $2$ ). Saturation profiles become steeper as  $\chi$  increases. Figure 2 shows the effects of the exponent of the velocity scaling law,  $\nu$ , on the spatial profiles  $s(x, t)$ : again, the profiles become steeper as  $\nu$  increases, although the variation is milder than for the  $\chi$  variation. In both cases, the agreement between Monte Carlo simulation and numerical integration of the corresponding equation is excellent.

In the context of underground contaminant transport, abrupt spatial variations in the physical properties of the traversed media may commonly arise [22,24]. These, in turn, give rise to sharply varying (i.e., possibly discontinuous) transport coefficients and strongly affect particles trajectories. We address one such case by considering a spatially discontinuous  $\kappa_0$ : in particular, we assume that at a given interface between two layers  $\kappa_0$  has a sudden step variation, while being constant in each layer separately. This situation is usually referred to as a macroscopic heterogeneity (the two layers are thought to be homogeneous at the local scale) [27]. All the other parameters are constant across the interface. The schemes (19) and (21) would be suitable to deal also with more involved cases, e.g., multiple heterogeneities. Recent experimental results [28] suggest that modeling transport through a sharp interface may require skewed flux corrections [29]. In this work, we do not address this issue and assume that the fluid flux is adequately described by Eq. (2), so that the random-walk schemes above hold. In Figs. 3 and 4, we display the breakthrough curves  $j_s(\ell, t)$  as a function of time and the spatial saturation profiles  $s(x, t)$  at a fixed time, respectively. We compare the curves for the case of fluid flow passing first through the layer at high  $\kappa_0=0.4$  and then through the layer at low  $\kappa_0=0.05$  with those where flow is in the opposite direction. For the boundary conditions considered here, fluid flow reaches the outlet earlier in the former case (Fig. 3). Remark that for the chosen boundary and initial conditions, the breakthrough curve reaches the saturation value  $j_s(\ell, t \rightarrow \infty) = v_0$ . The saturation profiles along the column show sharp gradients at the interface, while preserving continuity (Fig. 4). In both cases, the agreement between Monte Carlo simulation and numerical integration of the corresponding equation is excellent.

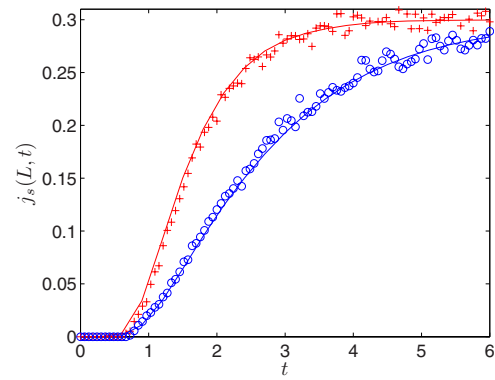


FIG. 3. (Color online) Breakthrough curves  $j_s(\ell, t)$  as a function of time  $t$  for discontinuous  $\kappa$  coefficient. The interface is located at  $x_d = \ell/2$ . Numerical integration is displayed as solid lines, Monte Carlo simulation as symbols:  $\kappa_0=0.4$  in the left layer and  $\kappa_0=0.05$  in the right layer (red crosses);  $\kappa_0=0.05$  in the right layer and  $\kappa_0=0.4$  in the left layer (blue circles). The other coefficients are  $\nu=0.2$ ,  $v_0=0.3$ , and  $\chi=0.1$ .

Note that for the case of nonconstant velocity  $v$ , the breakthrough curve  $j_s(\ell, t) = v(s)|_{x=\ell}$  does not coincide (up to a normalization constant) with the saturation  $s(\ell, t)$  measured at the outlet. This is immediately apparent from Fig. 5, where we show Monte Carlo simulations and numerical integrations of the two curves (for the same parameters). This point might be relevant while applying inverse problem techniques to the estimate of model parameters on the basis of experimental data.

Finally, in Figs. 6 and 7, we display the spatial profiles and the outlet values of the contaminant concentration, respectively, corresponding to a finite-duration step injection. The computed quantity is  $c(x, t)s(x, t)$ , i.e., the product of concentration and saturation. The spatial profiles are visibly skewed (Fig. 6) and this behavior is reflected in the long tail of the concentration measured at the outlet of the column as a function of time (Fig. 7). These features result from the coupling with the saturation and from the nonlinearities in-

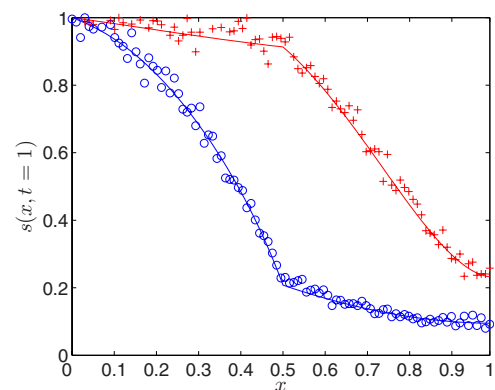


FIG. 4. (Color online) Saturation level spatial profiles  $s(x, t)$  at fixed time  $t=1$ . Numerical integration is displayed as solid lines, Monte Carlo simulation as symbols:  $\kappa_0=0.4$  in the left layer and  $\kappa_0=0.05$  in the right layer (red crosses);  $\kappa_0=0.05$  in the right layer and  $\kappa_0=0.4$  in the left layer (blue circles). The other coefficients are  $\nu=0.2$ ,  $v_0=0.3$ , and  $\chi=0.1$ .

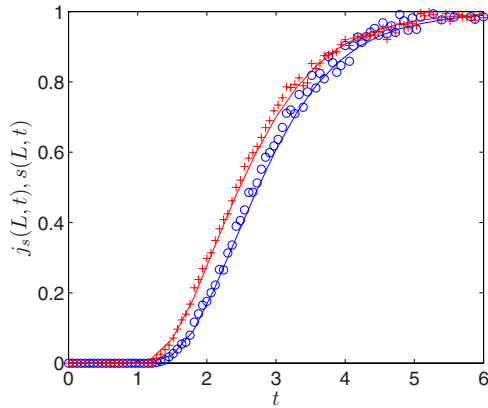


FIG. 5. (Color online) Breakthrough curve (blue circles) and saturation level (red crosses) at the column outlet, normalized so to have unit maximum. Solid lines correspond to numerical integration, symbols to Monte Carlo simulation. A discrepancy between the profiles is apparent for nonconstant velocities  $v$ . The coefficients are  $\kappa_0=0.05$ ,  $\nu=0.4$ ,  $v_0=0.3$ , and  $\chi=0.1$ .

involved in the flow-transport processes and could possibly explain the heavy-tailed breakthrough curves reported in the literature (see, e.g., [7]) for nonsaturated homogeneous porous media.

## V. FLUID FLOW THROUGH UNSATURATED HETEROGENEOUS MEDIA

So far, we have focused our attention on the case of unsaturated homogeneous porous materials, i.e., materials that do not display any significant degree of disorder in the pore-space geometry. The homogeneity hypothesis is mirrored in the Markovian nature of the associated random walks: all spatial sites are statistically equivalent and particle sojourns have the same duration  $\tau$  at each of them, so that trajectories have no memory of past positions. On the other hand, it is well known that porous media are actually characterized by heterogeneities at multiple scales, which ultimately affect

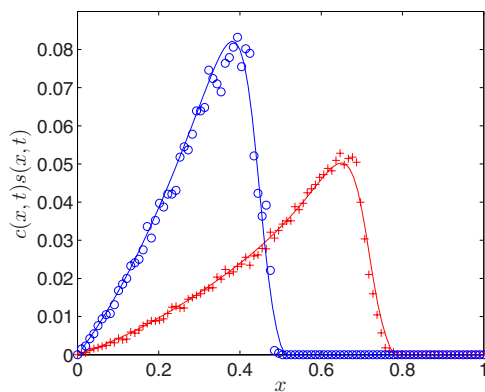


FIG. 6. (Color online) Contaminant concentration profiles  $c(x, t)s(x, t)$  at a fixed time  $t=1$ , for step injection from  $t_0=0$  to  $t_c=0.1$ . The simulation parameters are  $\kappa_0=0.05$ ,  $\chi=0.4$ ,  $v_0=0.3$ ,  $\nu=0.2$ ,  $D_0=0.1$ , and  $\phi=2$ . Monte Carlo simulations are shown as symbols (blue circles at  $t=0.5$ , red crosses at  $t=1$ ), numerical integration as solid lines.

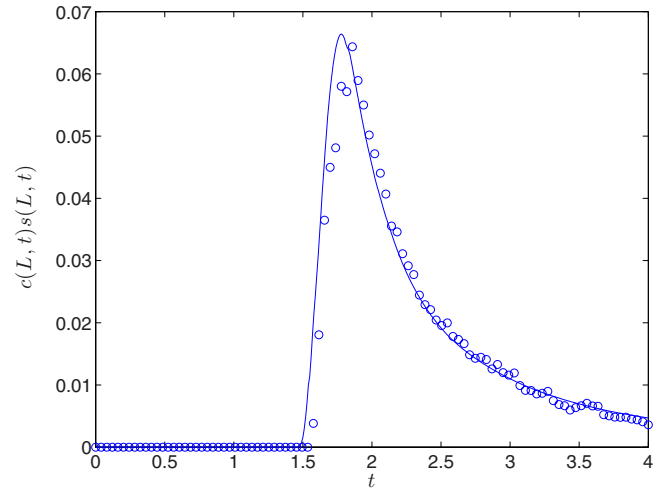


FIG. 7. (Color online) Contaminant profile  $c(\ell, t)s(\ell, t)$  measured at the column outlet, as a function of time, for step injection from  $t_0=0$  to  $t_c=0.1$ . The simulation parameters are  $\kappa_0=0.05$ ,  $\chi=0.4$ ,  $v_0=0.3$ ,  $\nu=0.2$ ,  $D_0=0.1$ , and  $\phi=2$ . Monte Carlo simulations are shown as symbols, numerical integration as solid line.

fluid and contaminant particles displacements [15,30].

Consider a fluid flow in a complex (possibly fractal) porous microgeometry. In such a situation, the fluid parcels tend to flow in preferential channels [20], so that the distribution of the sojourn times at each site is necessarily non-uniform, as suggested by experimental evidence [31]. A detailed account of Richards' equation inadequacy to explain a number of fluid flow experiments can be found in [18,32–34] and references therein. In recent years, some extensions of the Richards equation have been proposed to take into account these phenomena [16,18,35]. In particular, it has been conjectured that the wetting front in infiltration processes through nonhomogeneous aggregated media remains immobile for long-time periods and the structural hierarchy of the soil structure is a primary cause of non-Fickian dynamics [18,36]. An expedient means of incorporating such effects into the random walk described by Eq. (7) is to allow for the possibility of trapping events of random duration after each displacement (of duration  $\tau$ ). While several hypotheses can be made on the interplay between displacements and retention times, each corresponding to a distinct conceptual picture of the underlying physical system [13,37], here we follow the lines of a continuous time random-walk approach called fractal mobile-immobile model (f-MIM) [38], which suitably generalizes the discrete-time process defined by Eq. (7).

Within this framework, it is commonly assumed that trapping times between displacements obey “fat-tailed” (power-law) distributions  $\psi_s(t) \sim t^{-1-\alpha}$ ,  $\alpha > 0$ . If the decay is sufficiently slow, it is not possible to single out a dominant time scale (i.e., the mean of the pdf is not defined) and particles can thus experience a large variation of sojourn times, hence a broad spectrum of effective velocities at each spatial site [15]. Note that the precise functional shape and parameter values for  $\psi_s(t)$  should condense the fine details of the pore geometry and also of the internal repartition of the wetting fluid, in the case of unsaturated flow.

More precisely, assume

$$\psi_s(t) = \tau^{-1/\alpha} \psi(t/\tau^{1/\alpha}), \quad (24)$$

$0 < \alpha < 1$ , with  $\psi$  being a pdf concentrated on  $R^+$ , with survival probability  $\Psi(t) = \int_t^{+\infty} \psi(t') dt' = \lambda t^{-\alpha} / \Gamma(1-\alpha) + \mathcal{K}(t)$ ,  $\mathcal{K}$  being integrable. Here,  $\lambda \geq 0$  is a scaling factor that defines the strength of the trapping events. While in principle,  $\lambda$  could depend on  $x$ ,  $t$  [39] and even on the particles concentration, here, for sake of simplicity, we assume that it is constant.

Within the framework of the continuous-time random-walk models as applied to porous media, a power-law trapping times distribution is usually introduced on a phenomenological basis, so to allow fitting the slowly (i.e., power-law) decaying tails of experimentally measured breakthrough curves. Nonetheless, several attempts have been made over the years with the goal of providing a solid mathematical and physical justifications of the appearance of such distribution [8,15,18,40].

In particular, we expect that the geometrical structure of the domain occupied by water in an unsaturated medium can be very important. It will depend on the saturation, but also on the past history of the medium (wetting or drainage) [41]. After a previously saturated medium has been dried, small films of water are present everywhere. On the other hand, imbibition may result into an entirely wet connected subset, together with a dry connected subset [41]. In this case, the flow is mostly dominated by the more filled pores, but films where the flow velocity is very slow can retain the tracers. Even though such films are difficult to detect, electric conductivity measurements show that their impact may be significant [42]. At low saturations, these films negligibly contribute to hydraulic conductivity (hence to rapid mass transport), but significantly to the porous medium electric conductivity. As such, they can act as retention zones for both fluid parcels and tracer particles. These films may also occur in unsaturated media that are not especially heterogeneous from the macroscopic point of view, such as sand columns, where memory effects have been observed [7]. We nevertheless expect small-scale heterogeneities, related, e.g., to grain surfaces, to possibly influence the dynamics of fluid films [43]. Large-scale heterogeneities across distinct geological units also determine the distribution  $\psi(t)$  because of their different physical properties and/or flow conditions [8,29]. The complex interaction of all these phenomena ultimately affects the functional behavior of  $\alpha$  with respect to the geometrical and dynamical properties of the porous medium, a question that surely deserves further solid experimental and theoretical investigations.

Consider now the random walk defined by Eq. (7). At the end of each displacement, particles wait at the visited spatial site for a random time obeying the pdf  $\psi_s(t)$ : these sojourn times can be very long as compared to the time scale  $\tau$ . Because of trapping events, the number of jumps performed by each walker in a given time span may greatly vary: this is an effective means of describing heterogeneous media. We denote by  $P^m(x, t)$  and  $P^i(x, t)$  the densities of mobile and immobile fluid parcels, respectively, and by  $P = P^m + P^i$  the total density.

Let  $x_{j,n}$  be the position of walker  $j$  just after the  $n$ th step, which begins at time  $t_{j,n}$ . This ‘‘mobile’’ step is followed by the  $n$ th ‘‘immobile’’ period, with duration  $\tau^{1/\alpha} W_n$ , where the  $W_n$  are independent random variables drawn from  $\psi$  (so that the pdf of  $\tau^{1/\alpha} W_n$  is  $\psi_s$ ). Then we have

$$x_{j,n+1} = x_{j,n} + A\tau + \sqrt{2B\tau}\xi_n \quad (25)$$

and

$$t_{j,n+1} = t_{j,n} + \tau + \tau^{1/\alpha} W_n. \quad (26)$$

As a particular case, when  $\lambda=0$ , the second equation reduces to  $t_{j,n+1} = t_{j,n} + \tau$  plus a random contribution that vanishes in probability when  $\tau \rightarrow 0$  and we recover the homogeneous random walk defined by Eq. (7). When  $A$  and  $B$  are uniform and constant, in the hydrodynamic limit ( $\tau \rightarrow 0$ ), the particles dynamics above defines a linear fractal-MIM model [38,44], a generalization of the standard (linear) MIM model [45]. In this case, it can be shown via subordination that  $P$  satisfies an equation akin to Eq. (9), except that the left-hand side is replaced by  $[\partial_t + \lambda \partial_t^\alpha]P$ , with  $\partial_t^\alpha$  being a Caputo derivative of order  $\alpha$  [38] (details are provided in Appendix A).

Unsaturated flow in porous media can be characterized by droplets, slug-flows, Darcy’s flow, or all of the above. Correspondingly,  $A$  and  $B$  may depend on  $P$  or  $P^m$ . In highly unsaturated materials, we may conjecture that smaller pores, previously wetted and full of trapped fluid, modify the surface properties of larger pores where mobile fluid flows, so that  $A$  and  $B$  may depend also on  $P^i$ . For sake of simplicity, we have neglected here other possibilities: for instance, additional nonlinearities would be introduced at strong solutes concentrations [46]. In all such cases, it is more convenient to derive the governing equation for the fluid parcels density by resorting to the relation between  $P^m(x, t)$  and  $P^i(x, t)$  as in [44].

We make use of the ancillary pdf  $f(x, t)$  for a walker of just being released from a trap at  $x$ , at time  $t$ , and denote by  $r(x, t)$  a possible source term. Particles that are mobile at time  $t$  were either released from a trap or came from the source at time  $t-t'$ , with  $0 < t' < \tau$ . We assume that the diffusive step of the displacement occurs at the end of the mobile period (see the discussion in [39]). Moreover, during the time interval  $[t-t', t]$ , the motion of a walker is determined by the velocity field  $A$ : we denote the traveled distance by  $u_{x,t,t'}$ .

Hence, we have

$$P^m(x, t) = \int_0^\tau [f + r](x - u_{x,t,t'}, t - t') dt', \quad (27)$$

which implies

$$[f + r](x, u_{x,t,\tau}, t - \tau) = \tau^{-1} P_m(x, t) + O(\tau) \quad (28)$$

provided that  $A$  (hence  $u$ ) and  $f+r$  are smooth [47].

The density  $P^i$  also depends on  $f+r$ : any immobile particle at time  $t$  was trapped at a time  $t' < t$  at the end of a mobile step that began at time  $t-t'-\tau$  and involved a single diffusive step  $\sqrt{2B\tau}\xi$ . Denoting by  $y$  the amplitude of this latter step, we have

$$P^i(x,t) = \int_{y \in R} dy \int_0^t dt' \Psi(t'/\tau^{1/\alpha}) \varphi_{\sqrt{2B\tau}}(y) \times [f+r](x-y - u_{x-y,t-t',\tau} t - t' - \tau). \quad (29)$$

Here,  $\Psi(t'/\tau^{1/\alpha})$  represents the probability for a trapping duration to be larger than  $t'$  and  $\varphi_{\sqrt{2B\tau}}(y) = 1/\sqrt{2B\tau} \varphi(y/\sqrt{2B\tau})$  denotes the pdf of  $\xi$ ,  $\varphi$  being the normal distribution. Moreover,  $B$  may be nonuniform and depend on the starting point of each jump [ $x-y$  in Eq. (29)]. In the following, we will assume that  $A$  and  $B$  depend on  $(x,t)$  either directly or because they are functions of densities such as  $P^m$ ,  $P^i$ , or  $P$ . Bounded domains (such as those considered later in numerical simulations) are dealt with by setting absorbing boundary conditions. In the integrals over  $R$ , as in Eq. (29), this corresponds to letting the particle densities ( $f+r$ ,  $P^m$ , or  $P^i$ ) vanish at the exterior of the domain.

Denoting time convolutions (in  $R^+$ ) by  $*$ , i.e.,  $F*G(t) = \int_0^t F(t-t')G(t')dt'$ , and recalling that  $\Psi$  is bounded by 1, we make use of approximation (28) in Eq. (29) and obtain

$$P^i(x,t) = \tau^{-1} \Psi(t/\tau^{1/\alpha}) * \int_{y \in R} P^m(x-y,t) \varphi_{\sqrt{2B(x-y)\tau}}(y) dy + O(\tau). \quad (30)$$

In the hydrodynamic limit,

$$\int_{y \in R} P^m(x-y,t) \varphi_{\sqrt{2B(x-y)\tau}}(y) dy \rightarrow P^m(x,t)$$

(due to lemma 4 of Appendix C) and the (time) convolution of kernel  $\tau^{-1} \Psi(t/\tau^{1/\alpha})$  converges to the fractional integral  $\lambda I_{0,+}^{1-\alpha}$  (see Appendix A), hence

$$P^i(x,t) = \lambda I_{0,+}^{1-\alpha} P^m(x,t), \quad (31)$$

which provides a relation between  $P^m$  and  $P^i$ . We can identically rewrite as

$$P(x,t) = [\text{Id} + \lambda I_{0,+}^{1-\alpha}] P^m(x,t). \quad (32)$$

Then, the inversion of the term  $\text{Id} + \lambda I_{0,+}^{1-\alpha}$  yields [44]

$$P^m(x,t) = [\text{Id} + \lambda I_{0,+}^{1-\alpha}]^{-1} P(x,t). \quad (33)$$

The hydrodynamic limit of the walkers flux  $\mathcal{F}(x,t)$  [corresponding to the dynamics in Eqs. (25) and (26)] is derived in Appendix B and reads

$$\mathcal{F} = [A - \partial_x B] P^m. \quad (34)$$

This follows from the fact that particles contribute to the flow only when being in the mobile phase  $P^m$ . Finally, mass conservation  $\partial_t P = -\partial_x \mathcal{F} + r$  implies

$$\partial_t P = -\partial_x [A - \partial_x B] P^m + r, \quad (35)$$

which is the desired governing equation for transport processes with trapping events [48]. Equation (35), rather than being simply postulated as a phenomenological “fractional derivatives generalization” of the standard Richards equation, has been here derived as the hydrodynamic limit of an underlying nonlinear and non-Markovian stochastic process with a definite physical meaning. Remark that Eq. (35) is in

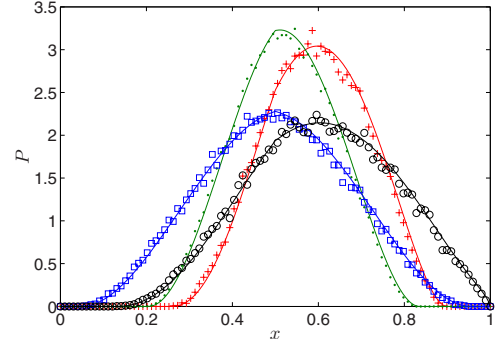


FIG. 8. (Color online) Unsaturated media with trapping processes: fluid flow profiles  $P$  at time  $t=2.25 \times 10^{-2}$ . For all curves,  $\alpha=0.6$  and  $\lambda=1$ . Red crosses:  $a_0=4$ ,  $a=0.25$ ,  $b_0=0.2$ ,  $b=0.5$ . Green dots:  $a_0=1$ ,  $a=0.25$ ,  $b_0=0.2$ ,  $b=0.5$ . Blue squares:  $a_0=0.1$ ,  $a=0.25$ ,  $b_0=0.5$ ,  $b=0.5$ . Black circles:  $a_0=5$ ,  $a=0.25$ ,  $b_0=0.5$ ,  $b=0.5$ . The corresponding numerical integration curves are plotted as solid lines.

principle nonlinear, as the coefficients  $A$  and  $B$  may depend on  $P$ ,  $P^m$ , or  $P^i$ , as is the case for unsaturated flows. Moreover, Eq. (35) contains a memory kernel [via the relation [32] between  $P^m$  and  $P$ ]: in other words, because of the slowly decaying time kernel, knowledge of the past history of the particle is required in order to determine its future displacement. Therefore, the fluid parcels density is affected at the same time by nonlinearities and memory effects: the relative strength of these components ultimately determines the fate of the flow in the traversed media.

Since Eq. (35) is written in a “Fokker-Planck form,” i.e., with a term of the kind  $\partial_x \partial_x B P^m$ , the corresponding conservative (Fickian) formulation for the flux would need the introduction of a drift coefficient correction,  $A$ , analogous to the one used for the standard Richards equation in homogeneous media.

The behavior of fluid flow with nonlinear coefficients and retention times is illustrated in Figs. 8 and 9. In particular, we proceed to compare the Monte Carlo simulations of the

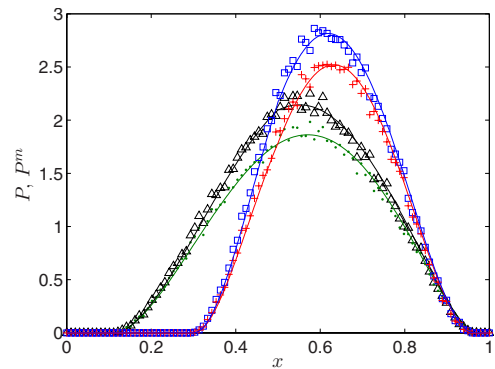


FIG. 9. (Color online) Unsaturated media with trapping processes: fluid flow profiles at time  $t=2.25 \times 10^{-2}$ . For all curves,  $\alpha=0.4$  and  $\lambda=1$ . Black triangles ( $P$ ) and green dots ( $P^m$ ):  $A = a_0(P^m)^a$  and  $B = b_0(P^m)^b$ , with  $a_0=2$ ,  $a=0.4$ ,  $b_0=0.4$ ,  $b=0.6$ . Blue squares ( $P$ ) and red crosses ( $P^m$ ):  $A = a_0(P)^a$  and  $B = b_0(P)^b$ , with  $a_0=6$ ,  $a=0$ ,  $b_0=0.2$ ,  $b=0.5$ . The corresponding numerical integration curves are plotted as solid lines.

random walks described by Eqs. (26) and (25) (in the hydrodynamic limit) to the numerical integration of the governing equations (31) and (35). Monte Carlo simulations proceed along the same lines as for homogeneous media. Concerning the numerical integration, we found more expedient to recast Eq. (35) in the equivalent formulation

$$[\partial_t + \lambda D_t^\alpha] P^m = -\partial_x[A - \partial_x B]P^m + r, \quad (36)$$

with  $D_t^\alpha$  being a Riemann-Liouville fractional derivative, defined in Appendix A. Once Eq. (36) has been solved for  $P^m$ ,  $P$  is easily computed from Eq. (32). We discretized Eq. (36) according to a semi-implicit scheme as in [44], so to avoid possible instabilities connected with nonlinearities.

In Fig. 8, we display the total fluid flow density  $P$  at a given time, for different values of the coefficients. We make the hypothesis that  $A$  and  $B$  depend on the mobile phase  $P^m$ , with a power-law scalings  $A = a_0(P^m)^a$  and  $B = b_0(P^m)^b$  (similarly as done for the homogeneous media). The initial condition is a fluid pulse located at  $x_0 = \ell/2$ . Absorbing boundary conditions are set at either end of the medium. In Fig. 9, we display the total fluid flow density  $P$  as compared to the mobile density  $P^m$ , when the parameters  $A$  and  $B$  separately depend (with a power-law scaling) on the mobile or total fluid density. Boundary and initial conditions are the same as in the previous example. Both figures show a very good agreement between Monte Carlo simulation and numerical integration.

Finally, replacing Eq. (24) with  $\psi_s(t) = \tau\psi(t/\tau)$  yields  $P^i = \lambda P^m$  when  $\psi$  has a finite average  $\lambda$ , i.e., when the pdf decays sufficiently fast at long times. In this case, Eq. (35) holds with  $P^m = (1 + \lambda)^{-1}P$  and we have

$$(1 + \lambda)\partial_t P = -\partial_x[A - \partial_x B]P + (1 + \lambda)r, \quad (37)$$

which is a nonlinear Fokker-Planck equation with a retardation factor  $\lambda$  [39].

## VI. DISCUSSION AND CONCLUSIONS

In this work, we have addressed nonlinear coupled flow and transport processes in variably saturated porous media. After briefly recalling the governing equations for homogeneous materials, we have shown how to describe fluid and solute parcel trajectories by resorting to a unified random-walk framework. Monte Carlo simulations of the underlying microscopic particle dynamics have been successfully compared to the numerical solutions of the governing equations.

We have then introduced a nonlinear f-MIM CTRW scheme aimed at describing fluid flow through variably saturated heterogeneous media. The effects of spatial heterogeneities are mirrored in the possibility of long (power-law distributed) sojourn times of the flowing particles at each visited site. The corresponding governing equations have been derived and their numerical integration has been then compared to the Monte Carlo simulations of the walkers dynamics. We remark that the proposed f-MIM generalization of nonlinear transport equations is not unique in any respect. Indeed, other possible approaches have been illustrated, e.g., in [49,50] and in [51] by means of a generalized Montroll-

Weiss master equation with a jump pdf depending on the walkers density.

Although focus has been given to fluid flow through heterogeneous unsaturated materials, the proposed nonlinear f-MIM scheme is fairly general and can be straightforwardly applied to the coupled solute-transport problem as well. Similarly, as fluid parcels can be affected by the irregular geometry of the traversed material, the solutes concentration can also experience the effects of inhomogeneities due, for instance, to the chemical-physical exchanges of the solute species with the surrounding environment [52]. In analogy with the case of fluid flow dynamics, we may then take into account these contributions by introducing a power-law distribution  $\psi_c(t) \sim t^{-1-\beta}$ , with  $\beta > 0$ , for the waiting times of contaminant particles between displacements. This pdf characterizes the sorption times of the transported species within the medium. In general, there is no reason to suppose that the exponent  $\beta$  coincides with  $\alpha$ . A similar distinction between flow- and solutes-induced retention times has been previously introduced in [15,52,53] within a (linear) CTRW framework.

In summary, the solutes concentration in heterogeneous variably saturated materials may display deviations from standard Fickian behavior due to three concurrent processes: (i) the space- and time-varying saturation profile within the medium (nonlinear effects), (ii) the spatial heterogeneities experienced by the fluid flow (memory effects), and (iii) the spatial heterogeneities experienced by the solutes (memory effects). As experimental data such as contaminant profiles or breakthrough curves are usually limited and/or affected by measurement noise, distinguishing the effects of spatial heterogeneities on flow and transport processes separately is an highly demanding task and many research efforts have been recently devoted to this aim (see, e.g., [52] and references therein). At present, it is therefore an open question whether these distinct contributions could be separately analyzed on the basis of measured data or rather described by an effective CTRW model: we will discuss in detail this topic in a forthcoming paper.

As a final remark, note that in this work we have confined our attention to the migration of nonreacting (passive) species. Nonetheless, all the random-walk algorithms introduced here could be easily extended so as to describe the transport of radionuclides by computing the decay time before simulating the particle trajectory [54].

## ACKNOWLEDGMENTS

A.C. was supported by a grant (Order No. 7220) from the Swiss National Cooperative for the Disposal of Radioactive Waste (Nagra), Wettingen, Switzerland: the support was provided to Berkeley Laboratory through the U.S. Department of Energy Contract No. DE-AC02-05CH11231. M.C.N. thanks the Groupement MoMaS, Modélisation Mathématique et Simulations numériques liées aux problèmes de gestion des déchets nucléaires (PACEN/CNRS, ANDRA, BRGM, CEA, EDF, and IRSN). We thank S. Finsterle and Ph. Montarnal for interesting scientific discussions.

## APPENDIX A: FRACTIONAL INTEGRALS AND DERIVATIVES

The fractional integral  $I_{0,+}^\alpha f$  of order  $\alpha > 0$  is

$$I_{0,+}^{\alpha}f(t) = \frac{1}{\Gamma(\alpha)} \int_0^t (t-t')^{\alpha-1} f(t') dt',$$

which is a generalization of the usual multiple integrals to arbitrary (positive) order [55,56]. The Caputo fractional derivative  $\partial_t^{\alpha}f$  of order  $n < \alpha < n+1$  is

$$\partial_t^{\alpha}f(t) = I_{0,+}^{n+1-\alpha} \partial_t^{n+1} f(t),$$

with  $n$  being an integer [55,57,58]. The Riemann-Liouville fractional derivative  $D_t^{\alpha}$  is instead defined as

$$D_t^{\alpha}f(t) = \partial_t^{n+1} I_{0,+}^{n+1-\alpha} f(t)$$

for  $n < \alpha < n+1$ . Note that the Riemann-Liouville derivative applies to slightly more general functions than Caputo's and when both can be applied (i.e., for differentiable functions  $f$ ), we have  $D_t^{\alpha}f(t) = \partial_t^{\alpha}f(t) + t^{-\alpha}f(0+)/\Gamma(1-\alpha)$  for  $0 < \alpha < 1$ .

In Sec. V, we use the following lemma:

*Lemma 1.* (i) Suppose  $\Psi$  is a positive valued, decreasing function defined on  $R^+$ , with  $\Psi(0)=1$  and  $\Psi(t)=t^{-\alpha}/\Gamma(1-\alpha)+\mathcal{K}(t)$ , with  $\mathcal{K}$  integrable and  $0 < \alpha < 1$ . Then, the convolution of kernel  $\tau^{-1}\Psi(t/\tau^{1/\alpha})$  converges to  $I_{0,+}^{\alpha}$  in  $L^p(R^+)$ , with  $1 \leq p \leq +\infty$ , when  $\tau \rightarrow 0$ .

(ii) If  $\Psi$  is integrable, then the convolution of kernel  $\tau^{-1}\Psi(t\tau^{-1})$  converges to  $\int_{R^+}\Psi(t)dt\text{Id}$ .

*Proof.* Due to the above definitions, the convolution of kernel  $\tau\Gamma(1-\alpha)^{-1}(t/\tau^{1/\alpha})^{-\alpha}$  is exactly  $I_{0,+}^{1-\alpha}$ . Moreover, the convolution of kernel  $\tau^{-1/\alpha}\mathcal{K}(t/\tau^{1/\alpha})$  [as a mapping of  $L^p(R^+)$ ] is an approximation to  $\int_{R^+}\mathcal{K}(t)dt\text{Id}$  [55,56], so that the convolution of kernel  $\tau^{-1}\mathcal{K}(t/\tau^{1/\alpha})$  tends to zero when  $\tau \rightarrow 0$  (due to  $\alpha < 1$ ), which proves point (i). Point (ii) is a direct consequence of the Refs. [55,56] concerning approximations to Id.

*Remark.* With  $\varphi_{\ell}(y)=1/\ell\varphi(y/\ell)$ , the space convolution [denoted by  $\star$ , with,  $f \star g(x) = \int_{R^+} f(x-x')g(x')dx'$ ] of kernel  $\varphi_{\ell}$  converges to Id when  $\ell \rightarrow 0$  [55,56], in  $L^p$ , and we have  $\varphi_{\ell} \star G(x) \rightarrow G(x)$  pointwise when  $G$  is a continuous function.

## APPENDIX B: PROBABILITY CURRENT

We would like to prove Eq. (34). Let us first introduce the probability current of the random walk defined by Eqs. (26) and (25). The current is the probability for a walker to cross a given point  $x$  to the right during a time interval  $dt$ , minus the probability of crossing to the left, divided by  $dt$ . Upon multiplication by the total number of walkers involved in the random walk, it yields the average number of particles that cross  $x$  per unit time.

Note that a walker that is not at the end of the current mobile period crosses  $x$  during  $[t-dt, t]$ , provided that it was released from the trap at time  $t-t'$  (with  $0 < t' < \tau$ ), between  $x-u_{x,t,t'}-A(x-u_{x,t,t'}, t-t')$  and  $x-u_{x,t,t'}$ , if  $A > 0$ . This occurs with probability

$$\begin{aligned} & \int_0^{\tau} [f+r](x-u_{x,t,t'}, t-t')A(x-u_{x,t,t'}, t-t')dt dt' \\ & \simeq P^m(x,t)A(x,t)dt, \end{aligned}$$

when  $\tau \rightarrow 0$ , and the walker crosses  $x$  in the direction (dic-

tated by the sign of  $A$ ). Moreover, a walker crosses  $x$  by a diffusive step directed to the right with probability  $\int_{y>0}(f+r)(x-y-u_{x,t,t'}, t-\tau)\Phi[y/\sqrt{2\tau B(x-y)}]dy$  per unit time, where  $\Phi(z) = \int_z^{+\infty} \varphi(y)dy$ . This latter probability approximates  $\tau^{-1} \int_{y>0} P^m(x-y, t)\Phi[y/\sqrt{2\tau B(x-y)}]dy$  when  $\tau \rightarrow 0$  due to Eq. (28). Collecting finally contributions of jumps to the left, the probability current of the random walk in Eqs. (26) and (25) is

$$\begin{aligned} P^m A(x,t) + \tau^{-1} \int_{y>0} P^m(x-y,t)\Phi[y/\sqrt{2\tau B(x-y)}] \\ - P^m(x+y,t)\Phi[y/\sqrt{2\tau B(x+y)}]dy. \end{aligned}$$

Appendix C shows that the above integral converges to  $-\partial_x B P^m \int_{R^+} y^2 \varphi(y)dy$  due to the rapid decrease at infinity of  $\varphi$  and  $\Phi$ . Hence, in the hydrodynamic limit, the probability current is given by Eq. (34).

## APPENDIX C: TECHNICAL LEMMA

The above result is obtained by applying lemma 2 below, with  $G(x \pm y) = P^m(x \pm y, t)$  recalling that  $P^m(z, t) = 0$  for  $z$  outside the studied domain  $D_0$ .

*Lemma 2.* Let  $\Phi$  be a differentiable function over  $R^+$ , with  $y\Phi(y)$  integrable. Suppose also that  $B$ , as a function of space, has a derivative  $B'$  satisfying  $|yB'(x+y)/B(x+y)| < 2$ , provided that  $x$  and  $x+y$  belong to the bounded domain  $D_0$ . Suppose then that  $G$  vanishes at the exterior of  $D_0$ , and has a bounded derivative, and set  $I_{\pm} = \tau^{-1} \int_{y>0} G(x \pm y)\Phi[y/\sqrt{2\tau B(x \pm y)}]dy$ . Then, the quantity  $-I_+ + I_-$  converges to  $-4\partial_x[G(x)B(x)] \int_0^{+\infty} z\Phi(z)dz$  when  $\tau \rightarrow 0$ .

*Remarks.* (i) When  $\varphi$  is an even function satisfying  $\varphi(z) = -\Phi'(z)$  for  $z > 0$ , we have  $4 \int_0^{+\infty} z\Phi(z)dz = \int_{R^+} z^2 \varphi(z)dz$ .

(ii) The condition for  $B$  in lemma 2 is very restrictive, more especially if we want to address infinite domains (which is not the case here). It can be significantly weakened on the basis of lemma 2, provided  $B'/B$  remains uniformly bounded.

*Proof of Lemma 2.* We first show that (i)  $-I_+ + I_-$  takes the form  $2\varepsilon^{-1} \int_0^{+\infty} F(\varepsilon z)\Phi(z)dz$ ,  $F$  being a derivable function satisfying  $F(0)=0$ . Then, (ii) we apply lemma 3 further below.

In view of (i), let us fix  $x$ . The hypotheses of the lemma allow for two changes of variables  $z = g_{\pm}(y)/\sqrt{2\tau}$  in  $I_+$  and  $I_-$ , with  $g_{\pm}(y) = y/\sqrt{B(x \pm y)}$ . The inverse of  $g_{\pm}$  is  $h_{\pm}$ , with

$$g'_{\pm}(y) = 1/\sqrt{B(x \pm y)} \{1 \mp yB'(x \pm y)/[2B(x \pm y)]\},$$

$$h'_{\pm}(Z) = \sqrt{B[x \pm h_{\pm}(Z)]} \left\{ 1 \mp \frac{h_{\pm}(Z)B'[x \pm h_{\pm}(Z)]}{2B[x \pm h_{\pm}(Z)]} \right\}^{-1},$$

and  $h_{\pm}(0) = 0$ . With these notations, set  $\varepsilon = \sqrt{2\tau}$  and

$$F(Z) = G[x - h_-(Z)]h'_-(Z) - G[x + h_+(Z)]h'_+(Z). \quad (C1)$$

Then, letting  $y = h_{\pm}(\varepsilon z)$  in  $I_{\pm}$  yields  $-I_+ + I_- = 2\varepsilon^{-1} \int_0^{+\infty} F(\varepsilon z)\Phi(z)dz$ .

Now, to apply lemma 3, note that  $F'(0) = -2G'(x)B(x) + G(x)[h''_-(0) - h''_+(0)]$  and that  $h''_{\pm}(Z) = a_{\pm} \pm b_{\pm}$ , with

$$a_{\pm} = \pm \frac{h'_{\pm}(Z)B[x \pm h_{\pm}(Z)]}{2\sqrt{B[x \pm h_{\pm}(Z)]}} \left\{ 1 \mp \frac{h_{\pm}(Z)B'[x \pm h_{\pm}(Z)]}{2B[x \pm h_{\pm}(Z)]} \right\}^{-1}$$

and

$$b_{\pm} = \frac{\sqrt{B[x \pm h_{\pm}(Z)]}}{\left\{ 1 \mp \frac{h_{\pm}(Z)B'[x \pm h_{\pm}(Z)]}{2B[x \pm h_{\pm}(Z)]} \right\}^2} \frac{c_{\pm}}{2B[x \pm h_{\pm}(Z)]^2},$$

with

$$c_{\pm} = h'_{\pm}(Z)BB'[x \pm h_{\pm}(Z)] \pm h_{\pm}h'_{\pm}(Z)BB'' \\ \times [x \pm h_{\pm}(Z)] \mp h_{\pm}(Z)h'_{\pm}(Z)B'^2[x \pm h_{\pm}(Z)].$$

This implies  $h''_{\pm}(0) = \pm B'(x)$ , so that  $F'(0) = -2(GB)'(x)$ . Hence, lemma 2 is a consequence of the lemma 3 below, which itself comes from lemma 3 in [39].

*Lemma 3.* Let  $\Phi$  be a bounded function, with  $y\Phi(y)$  inte-

grable over  $R^+$ . Then, for any integrable function  $F$ , differentiable at point 0 and satisfying  $F(0)=0$ , with  $F(y)/y$  uniformly bounded, the expression

$$\epsilon^{-1} \int_0^{+\infty} F(\epsilon z)\Phi(z)dz$$

converges to  $F'(0)\int_0^{+\infty} z\Phi(z)dz$ , when  $\epsilon \rightarrow 0$ . In Sec. V, we make use of the following statement.

*Lemma 4.* Let  $G$  be a continuous bounded function, vanishing at the exterior of the bounded domain  $D_0$ ,  $\varphi$  being a pdf. Suppose also that  $B$  is as in lemma 2. Then,  $I = \int_R G(x-y)\varphi[y/\sqrt{2\tau B(x-y)}]dy/\sqrt{2\tau B(x-y)} \rightarrow G(x)$  when  $\tau \rightarrow 0$ .

As in the proof of lemma 2, the change of variables  $g(y) = y/\sqrt{B(x-y)}$  has an inverse, which we denote by  $h$ . Thus, we have  $I = \int_R G[x-h(\sqrt{2\tau z})]\varphi(z)dz$ . Hence, the remark of Appendix A proves the statement.

- 
- [1] M. Muskat, *The Flow of Homogeneous Fluids Through Porous Media* (McGraw Hill, New York, 1937).
- [2] R. Hilfer, *Adv. Chem. Phys.* **92**, 299 (1996).
- [3] J. Bear, *Dynamics of Fluids in Porous Media* (American Elsevier, New York, 1972).
- [4] M. Sahimi, *Flow and Transport in Porous Media and Fractured Rock* (VCH, Weinheim, 1995).
- [5] G. De Marsily, *Quantitative Hydrogeology, Groundwater Hydrology for Engineers* (Academic Press, New York, 1986).
- [6] A. Cortis and C. Knudby, *Water Resour. Res.* **42**, W10201 (2006).
- [7] M. Bromly and C. Hinz, *Water Resour. Res.* **40**, W07402 (2004).
- [8] M. Levy and B. Berkowitz, *J. Contam. Hydrol.* **64**, 203 (2003).
- [9] F. Delay, P. Ackerer and C. Danquigny, *Vadose Zone J.* **4**, 360 (2005).
- [10] M. Buecker-Gittel, U. Mohrlök, and G. H. Jirka, IAHS-AISH Publication No. 277, 2003, pp. 17–21.
- [11] M. Magdziarz, A. Weron, and K. Weron, *Phys. Rev. E* **75**, 016708 (2007).
- [12] R. N. Bhattacharya, V. K. Gupta, and G. Sposito, *Soil Sci. Soc. Am. J.* **40**, 465 (1976); **40**, NP-a (1976).
- [13] R. Metzler and J. Klafter, *Phys. Rep.* **339**, 1 (2000).
- [14] H. Scher and M. Lax, *Phys. Rev. B* **7**, 4491 (1973).
- [15] B. Berkowitz, A. Cortis, M. Dentz, and H. Scher, *Rev. Geophys.* **44**, RG2003 (2006).
- [16] E. Gerolymatou, I. Vardoulakis, and R. Hilfer, *J. Phys. D* **39**, 4104 (2006).
- [17] L. A. Richards, *Phys.* **1**, 318 (1931).
- [18] Y. Pachepsky, D. Timlin, and W. Rawls, *J. Hydrol.* **272**, 3 (2003).
- [19] A. Cortis and B. Berkowitz, *Soil Sci. Soc. Am. J.* **68**, 1539 (2004); **69**, 285 (2005).
- [20] C.-H. Park, C. Beyer, S. Bauer, and O. Kolditz, *Geosci. J.* **12**, 285 (2008).
- [21] H. Risken, *The Fokker-Planck Equation*, 2nd ed. (Springer, Berlin, 1989).
- [22] E. M. LaBolle, J. Quastel, G. E. Fogg, and J. Gravner, *Water Resour. Res.* **36**, 651 (2000).
- [23] E. M. LaBolle, J. Quastel, and G. E. Fogg, *Water Resour. Res.* **34**, 1685 (1998).
- [24] G. J. M. Uffink, *Proceedings of the Hamburg Symposium, August, 1983* (IAHS, Institute of Hydrology, Wallingord, UK1985), pp. 103–114.
- [25] R. H. Brooks and A. T. Corey, *J. Irrig. Drain.* **92**, 61 (1966).
- [26] M. T. Van Genuchten, *Soil Sci. Soc. Am. J.* **44**, 892 (1980).
- [27] A. Cortis, C. Gallo, H. Scher, and B. Berkowitz, *Water Resour. Res.* **40**, W04209 (2004).
- [28] B. Berkowitz, A. Cortis, I. Dror, and H. Scher, *Water Resour. Res.* **45**, W02201 (2009).
- [29] A. Cortis and A. Zoia, *Phys. Rev. E* **80**, 011122 (2009).
- [30] H. Scher, G. Margolin, and B. Berkowitz, *Chem. Phys.* **284**, 349 (2002).
- [31] R. Kimmich, *Chem. Phys.* **284**, 253 (2002).
- [32] S. C. Taylor, W. D. Hoff, M. A. Wilson, and K. M. Green, *J. Mater. Sci. Lett.* **18**, 1925 (1999).
- [33] M. Küntz and P. Lavalée, *J. Phys. D* **34**, 2547 (2001).
- [34] A. El-G. El Abd and J. J. Milczarek, *J. Phys. D* **37**, 2305 (2004).
- [35] Y. Pachepsky, D. Timlin, and W. Rawls, *J. Hydrol.* **279**, 290 (2003).
- [36] D. Or and T. A. Ghezzehei, *Transp. Porous Media* **68**, 129 (2007).
- [37] R. Metzler, E. Barkai, and J. Klafter, *Phys. Rev. Lett.* **82**, 3563 (1999).
- [38] R. Schumer, D. A. Benson, M. M. Meerschaert, and B. Baumer, *Water Resour. Res.* **39**, 1296 (2003).
- [39] M. C. Néel, A. Zoia, and M. Joelson, *Phys. Rev. E* **80**, 056301 (2009).
- [40] A. Cortis, Y. Chen, H. Scher, and B. Berkowitz, *Phys. Rev. E* **70**, 041108 (2004).
- [41] H. Ovdad and B. Berkowitz, *Adv. Water Resour.* **30**, 2373 (2007).

- [42] M. Han, S. Youssef, E. Rosenberg, M. Fleury, and P. Levitz, *Phys. Rev. E* **79**, 031127 (2009).
- [43] P. Beltrame, P. Hänggi, and U. Thiele, *EPL* **86**, 24006 (2009).
- [44] B. Maryshev, M. Joelson, D. Lyubimov, T. Lyubimova, and M. C. Néel, *J. Phys. A: Math. Theor.* **42**, 115001 (2009).
- [45] M. Th. Van Genuchten and P. J. Wierenga, *Soil Sci. Soc. Am. J.* **40**, 473 (1976).
- [46] A. Zoia, C. Latrille, and A. Cartalade, *Phys. Rev. E* **79**, 041125 (2009).
- [47] This is true when assuming that the term  $f+r$  has bounded derivatives (with respect to  $x$  and  $t$ ), dominated by  $t^{-1-\varepsilon}$  with  $\varepsilon > 0$ . This strong assumption implies that applying a time convolution with a bounded kernel will preserve the approximation (28). This was not necessary in [39], where only time-dependent velocity fields were addressed.
- [48] Another formulation, equivalent when parameters are constant, is  $(\partial_t + \lambda \partial_t^\alpha)P = -\partial_x[A - \partial_x B]P + (\text{Id} + \lambda I_{0,+}^{1-\alpha})r - \lambda t^{-\alpha}/\Gamma(1-\alpha)P^0$  [38].
- [49] R. Sánchez, B. A. Carreras, and B. Ph. van Milligen, *Phys. Rev. E* **71**, 011111 (2005).
- [50] B. Ph. van Milligen, R. Sánchez, and B. A. Carreras, *Phys. Plasmas* **11**, 2272 (2004).
- [51] J. F. Lutsko and J. P. Boon, *Phys. Rev. E* **77**, 051103 (2008).
- [52] B. Berkowitz, S. Emmanuel, and H. Scher, *Water Resour. Res.* **44**, W03402 (2008).
- [53] A. Cortis, T. Harter, L. Hou, E. R. Atwill, A. Packman, and P. Green, *Water Resour. Res.* **42**, W12S13 (2006).
- [54] A. Zoia, *Phys. Rev. E* **77**, 041115 (2008).
- [55] S. G. Samko, A. A. Kilbas, and O. I. Marichev, *Fractional Integrals and Derivatives: Theory and Applications* (Gordon and Breach, New York, 1993).
- [56] B. Rubin, *Fractional Integrals and Potentials* (Longman, Harlow, 1996).
- [57] A. A. Kilbas, H. M. Srivastava, and J. J. Trujillo, *Theory and Applications of Fractional Differential Equations*, North-Holland Mathematical Studies 204 (Jan van Mill, Amsterdam, 2006).
- [58] F. Mainardi, in *Fractals and Fractional Calculus in Continuum Mechanics*, edited by A. Carpinteri and F. Mainardi, CISM Courses and Lectures 378 (Springer, New York, 1997), pp. 291–348.